Chapter-6
Potentiodynamic Corrosion Behavior of Fe-18Cr-21Mn-0.65N Austenitic Stainless Steel

6.1 Introduction

In the previous chapter, it was shown that the mechanical properties such as tensile strength and ductility of the present grade of austenitic stainless steel are not much affected after exposure in air up to 100 h below 500℃. This opens a new realm for application of this material at intermediate temperatures. It is evident from our study in Chapter 3 that alloys of this class are susceptible to precipitation at temperatures above 500℃. The shape, amount and type of the chromium nitride precipitates formed, also influence corrosion resistance of these alloys. The study carried out by K. Krishna Kumar et al. [80] shows that aging at 700, 800, and 900℃ for 14 h causes precipitation of chromium nitrides. With increase in temperature, quantity of lamellar nitrides increases. They found that at 800 and 900℃ pitting resistance was higher and disc-shaped nitrides resisted pitting. The study carried out by Xinqiang Wu et al.[15] shows that compared to 316L, high nitrogen nickel free stainless steel shows higher resistance against pitting. Another study by Norman Kauss et al. [82] shows that Fe-Cr-Mn-N austenitic stainless steel performed better in terms of mechanical properties and pitting resistance. They also concluded that if the possibility of sensitization during use is ruled out then this class of alloys can be considered better than conventional austenitic stainless steel. Cl^- ions are inevitable in various industries such as fossil, food, paper, and chemical industry [143]. Stainless steel components have been widely used in such industries and exposed to seawater environment in the coastal region. This chapter deals with potentiodynamic polarization behavior of the Fe-18cr-21Mn-0.65N austenitic stainless steel, pre exposed at 400-700℃, up to 100 h, in seawater environment (0.5M NaCl). Polarization test shows that increase in exposure temperature reduced corrosion resistance of the steel. EIS study of the passive layer formed, also showed decreasing trend in corrosion resistance of surface barrier film. The corroded surface of the samples were characterized by X-ray photoelectron spectroscopy (XPS) and Scanning electron microscopy (SEM-EDS) techniques. XPS analysis revealed presence of oxides and

hydroxide of Cr^{+3}, Mn^{+3} and Fe^{+3}. Higher temperature of exposure in air caused formation of manganese hydroxide. Pitting was prominent from room temperature to 500°C while at higher temperatures of 600 and700℃, a mixed mode of intergranular corrosion and accelerated pitting was observed. Precipitation of Cr_2N along grain boundaries and within grains was found to be the main cause of the accelerated corrosion attack.

6.2. Results

6.2.1 EIS analysis

Figure 6.1 shows electrochemical impendence spectroscopy plots of the Fe-18Cr-21Mn-0.65N austenitic stainless steel of the unexposed and also exposed at 400-700℃ for 100 h, tested in 0.5M NaCl solution. EIS analysis is reported only for the samples which showed the highest corrosion current density, the samples that are exposed for 100 h duration at all temperatures. As described in Chapter 2, EIS measurement was carried out at open circuit potential. **Figure 6.1a**, **b** and **c** show the Nyquist and Bode plots of the samples exposed at different temperatures. It is clear from **Figure 6.1** that impedance curve of the unexposed sample as well of the samples exposed at different temperatures are unfinished semicircles. The size of the semicircle represents the amount of resistance offered during the charge transfer. The radius of the capacitive arc decreases with increasing the temperature of exposure, which shows decrease in the ability of passive layer to protect the alloy from corrosion. For better understanding of behavior of passive layer, EIS data were analyzed using equivalent electrical circuit as shown in **Figure 6.2**. The equations used for fitting the data are given elsewhere [144] and the parameters obtained from fitting of EIS data are listed in Table 6.1. R_1 is solution resistance, Q is constant phase element related to capacitance of the passive film and R_2 is resistance of passive film.

On analyzing the fitted data, it can be seen that as the temperature of exposure increases, R_2 for unexposed sample, it was 10025 Ωcm^2 and decreased to 3517 Ωcm^2 from exposure

at 700°C, the capacitance value also increases with increase in pre-exposure temperature, which shows that increase in total charge carrier in passive film.

Table 6.1: Electrochemical impedance spectroscopy (EIS) fitted parameters of Fe-18Cr-21Mn-0.65N austenitic stainless steel samples unexposed and exposed at 400-700°C.

Exposure temperature T (°C)	**R_1** (Ωcm^2)	**Q** ($\Omega . cm^{-2}s^n$)	**n**	**R_2** (Ωcm^2)
Unexposed	38.23	5.6×10^{-6}	0.75	10025
400	23.94	7.9×10^{-6}	0.76	9283
500	30.01	3.3×10^{-5}	0.73	6058
600	24.16	3.23×10^{-5}	0.83	5951
700	22.73	3.1×10^{-5}	0.83	3517

Note: EIS measurement was carried out at room temperature.

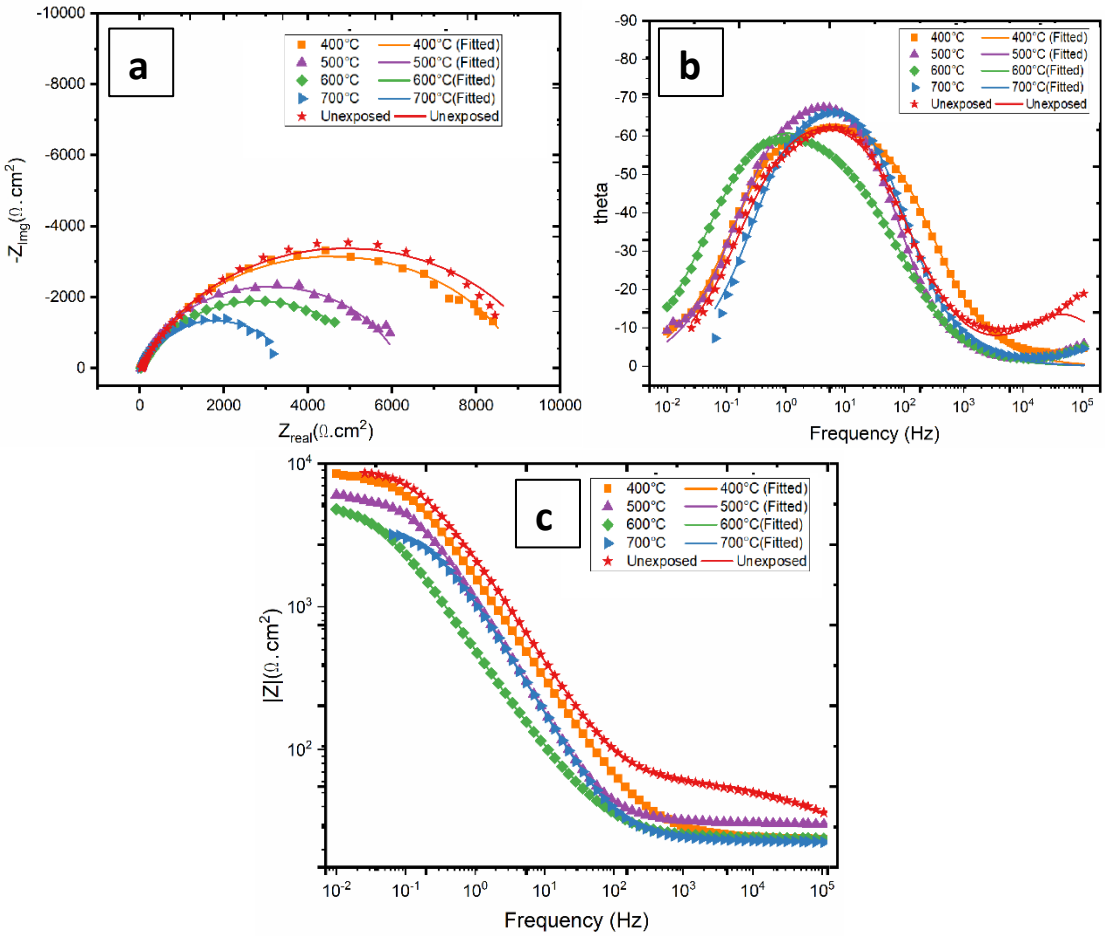

Figure 6.1: (a) Nyquist and (b, c) Bode plots of Fe-18Cr-21Mn-0.65N austenitic stainless steel samples, unexposed and exposed for 100 h at 400-700°C.

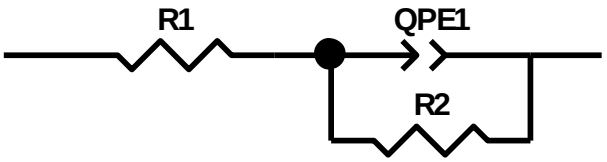

Figure 6.2: Equivalent circuit diagram used for fitting EIS data of Fe-18Cr-21Mn-0.65N austenitic stainless steel samples unexposed and exposed at 400-700℃ for 100 h.

Table 6.2: Polarization test parameters of Fe-18Cr-21Mn-0.65N austenitic stainless steel samples unexposed and exposed at 400-700℃ for different time intervals.

Temp. (℃)	Time (h)	i_{corr} (μA/cm^2)	±Error (μA/cm^2)	E_{corr} (V)	±Error (V)	CR (μm/year)	±Error (μm/year)
Unexposed	0	1.7	0.06	-0.190	0.011	0.19	0.006
400	5	1.4	0.08	-0.242	0.015	0.15	0.008
	50	3.8	0.3	-0.295	0.071	0.42	0.031
	100	7.9	0.33	-0.279	0.202	0.88	0.036
500	5	9.9	0.3	-0.336	0.023	1.10	0.030
	50	18.5	0.4	-0.379	0.028	2.05	0.041
	100	50.1	0.7	-0.434	0.011	5.54	0.076
600	5	16.8	0.32	-0.322	0.012	1.87	0.036
	50	44	0.9	-0.338	0.022	4.87	0.094
	100	91	0.9	-0.424	0.009	10.06	0.097
700	5	18.5	0.5	-0.309	0.006	2.053	0.051
	50	26.4	2.1	-0.364	0.022	2.93	0.247
	100	693.3	21.8	-0.414	0.004	76.67	2.417

Note: The polarization test was carried out at room temperature.

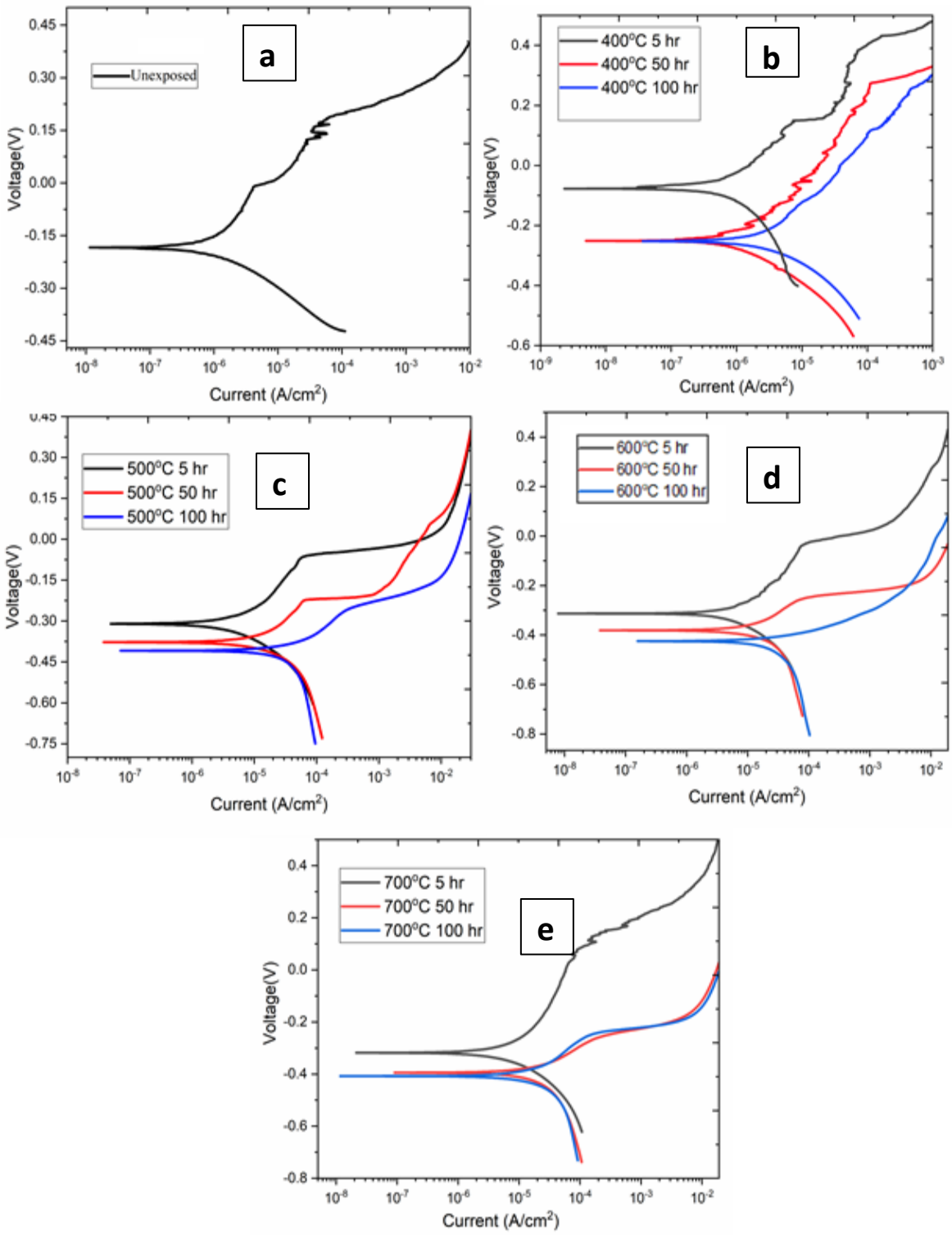

Figure 6.3: Potentiodynamic polarization plots of the Fe-18Cr-21Mn-0.65N austenitic stainless steel samples: (a) unexposed, and exposed at (b) 400°C, (c) 500°C, (d) 600°C, (e) 700°C for varying duration.

6.2.2 Polarization Test

Potentiodynamic polarization curve of the18Cr-21Mn-0.65N-Fe austenitic stainless with varying time and temperature of exposer is shown in **Figure 6.3**.

Unexposed sample

Figure 6.3a shows the potentiodynamic polarization plot of the unexposed sample. From the graph, it is clear that this steel does not exhibit any passive behavior, since a clear demarcation of the passive zone was not observed in chloride environment. The corrosion rate of the unexposed samples was 0.19 µm/year.

Exposed at 400°C

Figure 6.3 b shows the potentiodynamic polarization curve for samples exposed at 400°C with different duration of exposure. It can be observed that increase in exposure time at particular temperature, increases i_{corr}. Current densities of different exposure time were of similar order and were highest for 100 h exposure time (7.9±0.33µA/cm^2). The E_{corr} value of the samples exposed was lowest at 5 and 50 hr. The corrosion rate was highest for the sample exposed for 100 h (0.88 µm/year) and lowest for the sample exposed for 5 h (0.15 µm/year).

Exposed at 500°C

Potentiodynamic polarization plots of the samples exposed at 500°C for different time is shown in **Figure 6.3 c**. Current density of the sample exposed for 5 h was lowest (9.9±0.3µA/cm^2); however, with increase in exposure time to 100h, the current density increases almost by 5 times. E_{corr} values increases with time of exposure showing, decrease in corrosion resistance with time of exposure. Corrosion rate was highest for 100 h exposure (5.5 µm/year) and lowest for 5 h exposure time (1 µm/year).

Exposed at 600°C

Figure 6.3 d shows potentiodynamic corrosion plots of the samples exposed at 600°C for varying time. As time of exposure increases i_{corr} and E_{corr} increase. As observed at lower temperatures exposure (400 and 500°C), current density was lowest at 5 h of exposure ($16.8\pm0.32\mu A/cm^2$) and it increased almost eight times to $90\pm0.9\mu A/cm^2$ at 100 h of exposure. The sample exposed for 5 h exposure does not show any distinct pitting region. Corrosion rate was highest for the sample exposed for 100 h (10 µm/year) and lowest for the 5 h exposed sample (1.8 µm/year).

Exposed at 700°C

Figure 6.3 e shows the potentiodynamic corrosion plots of the samples exposed at 700°C for varying durations of exposure. At 5 h of exposure, current density was lowest ($18.5\pm0.5\mu A/cm^2$), which markedly increases for the 100h exposure to $693.3\pm21.8\mu A/cm^2$. There was almost one order of increase in current density, suggesting higher corrosion rate for longer exposure. The corrosion rate was highest of the sample exposed for 100 h (76 µm/year).

6.2.3 Surface layer analysis

6.2.3.1 XRD analysis

Figure 6.4 shows XRD patterns of the unexposed and exposed samples at 400-700°C for 100 h. Cr_2N peak can be seen in the sample exposed at 700°C for 100 h, in the inset. In unexposed and the samples exposed at 400-600°C, austenite phase may be seen prominent.

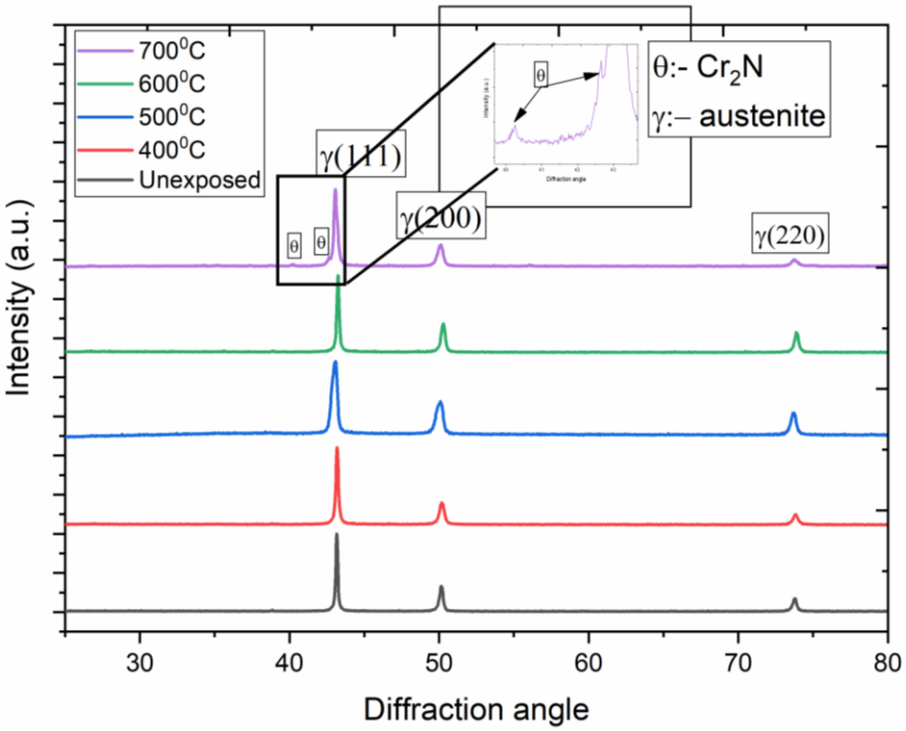

Figure 6.4: XRD patterns of the unexposed sample and the samples exposed at 400-700℃ for 100 h.

6.2.3.2 XPS (X-ray Photoelectron Spectroscopy)

The compositions of the passive film on the unexposed sample of Fe-18Cr-21Mn-0.65N austenitic stainless steel and those exposed in the temperature range of 400-700℃, for 100 h, after potentiodynamic corrosion test in 0.5 M NaCl, were analyzed by X-ray photoelectron spectroscopy.

Manganese

The Mn $2p_{3/2}$ spectra (**Figure 6.5 (a-e)**) shows that Mn^0(638.6eV), Mn^{+2} for MnO (640.2 eV) and Mn^{+3} for Mn_2O_3 oxide (640.8, 641.9 and 643.1eV) while for Mn^{+3} hydroxyl or MnOOH (640 eV, 641.7 eV, 642.5 eV and 643.5 eV) was present in the passive film in combination with other oxides of matrix elements [145-147]. The binding energies corresponding to these peaks were determined with ±0.5eV accuracy. At surface of the unexposed sample, only Mn_2O_3 is present while with increase in the exposure temperature occurrence of hydroxyl group increased. In the sample exposed at 400℃ for 100 h,

presence of MnOOH shows beginning of dissolution of oxides of Mn in the passive layer. Increase in the temperature to 500℃ shows considerable increase in MnOOH and for sample exposed at 600℃ only MnOOH was present. On the samples exposed at 700℃ for 100 h, Mn^0, Mn_2O_3 and MnOOH were detected.

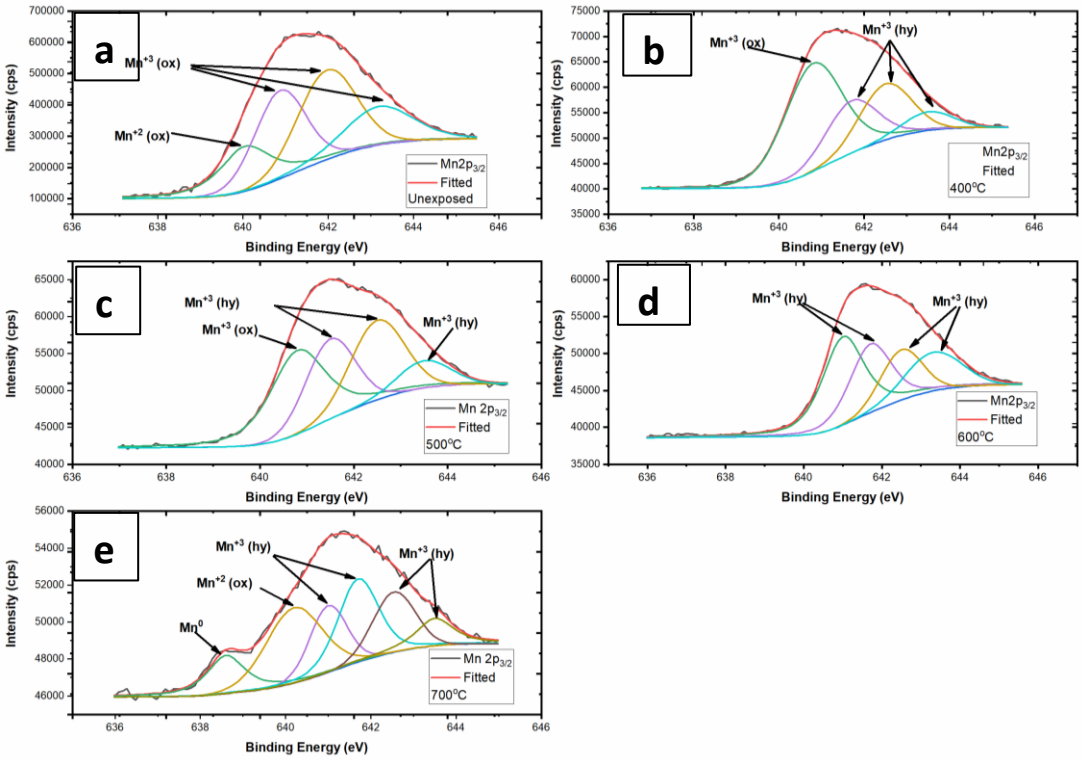

Figure 6.5: XPS plots of Mn $2p_{3/2}$ after polarization test of the Fe-18Cr-21Mn-0.65N austenitic stainless steel samples (a) unexposed, and exposed for 100h at (b) 400℃, (c) 500℃ (d) 600℃ and (e) 700℃.

Iron (Fe)

Figure 6.6 (a-e) shows the Fe $2p_{3/2}$ spectra where Fe^{+3}(709.8 eV and 710.8 eV) for Fe_2O_3 and for FeOOH (713.3), Fe^{+2} for FeO (708.4 eV) and Fe^0 (706.6 eV) are the main components of the passive film formed on the surface of all the specimens unexposed as well as exposed for 100h, from 400-700℃ [145, 148-150]. On surface of the unexposed sample Fe^{+3} was detected, which shows the presence of Fe_2O_3, at higher binding energies, presence of FeOOH was also observed; however, the amount of Fe_2O_3 was higher as compared to FeOOH, which shows stable nature of the passive layer. Similar trend was

observed for the samples exposed at 400 and 500°C for 100 h. In the samples exposed at 600 and 700°C for 100 h, presence of Fe^{+2} can be seen with Fe^{+3} oxides and hydroxides. In the samples exposed at 700°C, presence of metallic iron (706.68 eV) was observed which shows the extensive dissolution of the passive layer.

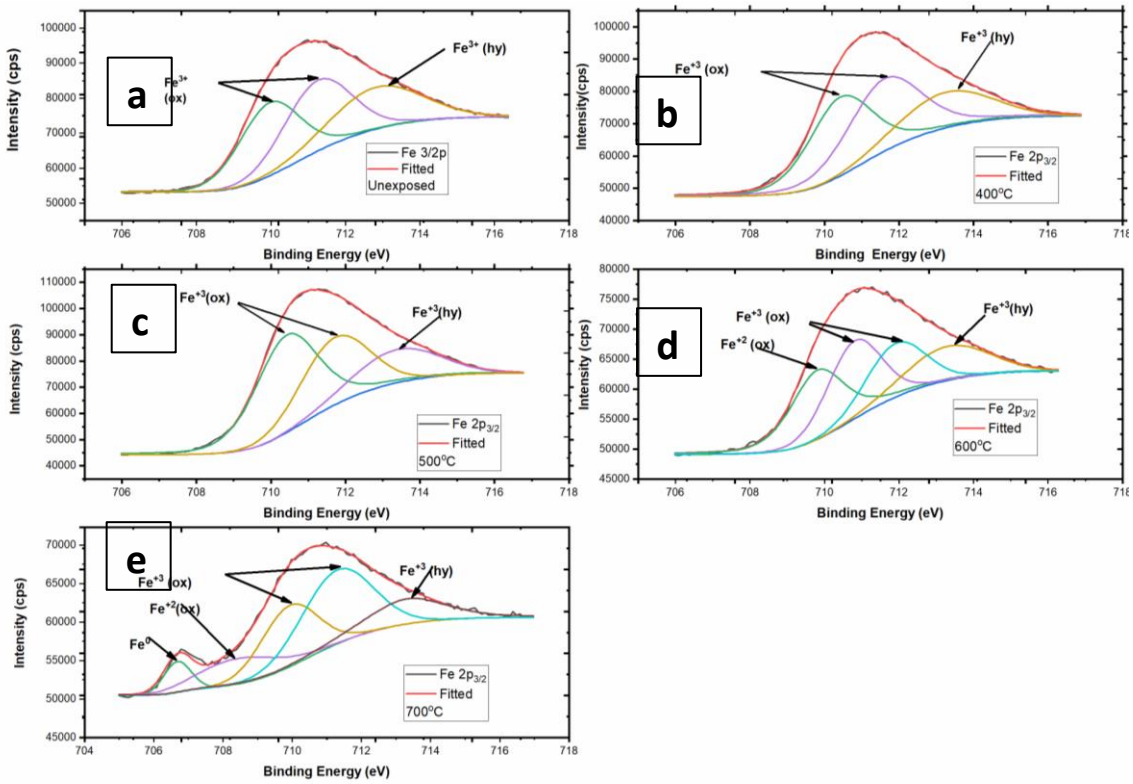

Figure 6.6: XPS plots of Fe $2p_{3/2}$ after polarization of Fe-18Cr-21Mn-0.65N austenitic stainless steel samples (a) un*expos*ed and exposed at (b) 400°C, (c) 500°C (d) 600°C and (e) 700°C for 100 h.

Chromium

Figure 6.7 (a-e) shows Cr $2p_{3/2}$ spectra and presence of Cr^0(574.2 eV), Cr^{+3} for Cr_2O_3 (575.7, 576.7, 577.5 and 578.5 eV), $Cr(OH)_3$ (577.3 eV) and Cr^{+6} (579.6 eV) in the passive film, in combination with other oxides of matrix elements [147, 148, 151]. The chromium oxide and hydroxide layer were prominent at all the samples exposed at different temperatures. In sample unexposed and those exposed at 400°C Cr_2O_3 formation was prominent. As temperature of exposure increased from 500 to 700°C, presence of $Cr(OH)_3$ can be seen, which signifies the dissolution of the Cr from the passive layer. Metallic

chromium peak was observed in the specimens exposed at 700°C along with chromium oxide and hydroxide and indicating excessive dissolution of passive layer formed at 700°C.

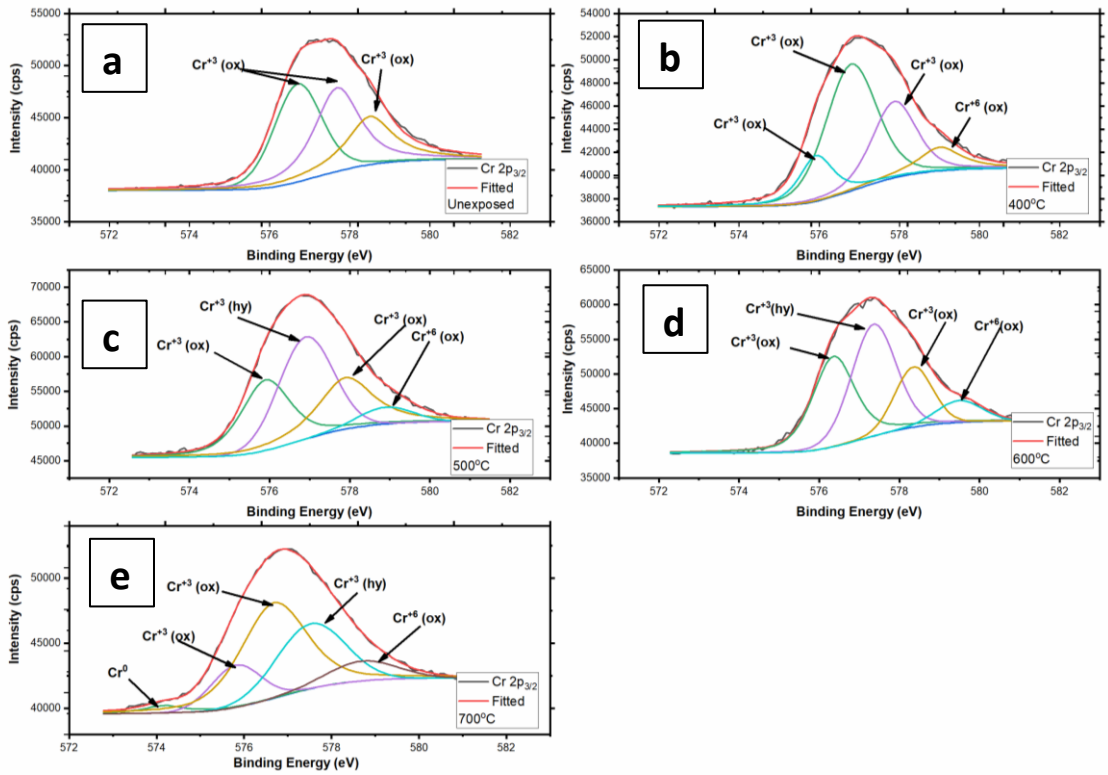

Figure 6.7: XPS plots of Cr $2p_{3/2}$ after polarization test of the Fe-18Cr-21Mn-0.65N austenitic stainless steel samples (a) unexposed, and exposed at (b) 400°C, (c) 500°C (d) 600°C and (e) 700°C for 100 h.

Oxygen

Figure 6.8 (a-e) shows O 1s spectra, reflecting the presence of oxygen in form of O^{2-}(529.7 eV), OH^-(531.2 eV) and H_2O (532.4 eV) [145, 148, 152]. The spectra were similar at all temperatures of exposure but there was difference in intensities of oxides and hydroxides. Unexposed samples show a distinct shoulder peak of O^{-2} while the amount of hydroxide was higher. Trends were similar for samples exposed at 400°C but the amount of hydroxide and oxide decreases. For samples exposed at 500°C for 100 h, intensity of O^{-2} decreases sharply, which shows that dissolution of oxides increased at this temperature. For samples exposed at 600 and 700°C similar trend was followed, while oxygen content at 700°C was highest compared to all other temperatures.

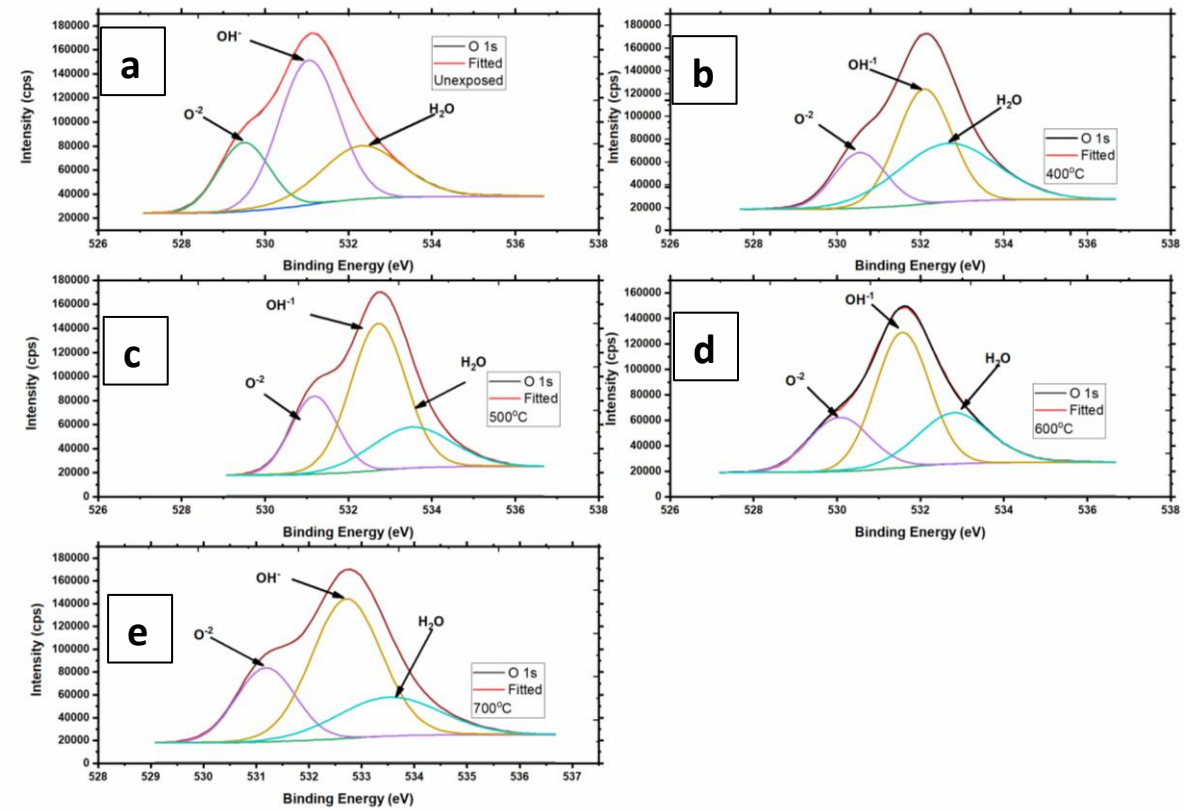

Figure 6.8: XPS plots of O 1s after polarization test of Fe-18Cr-21Mn-0.65N austenitic stainless steel samples (a) unexposed and those exposed at (b) 400°C, (c) 500°C (d) 600°C and (e) 700°C for 100 h.

6.2.3.3 SEM-EDS analysis

6.2.3.3.1 Surface analysis

Unexposed sample

Figure 6.9 a shows SEM-EDS analysis of the unexposed sample corroded in 0.5M NaCl solution. It shows presence of a few pits on surface. SEM micrograph shows that the pits were irregular in shape and diameter was around ~25µm. EDS from the bottom of the pit shows presence of oxygen and chlorine in small amount with other matrix elements.

Exposed at 400°C

Samples exposed at 400°C for 100 h show the formation of circular pits (diameter ~45µm) with small pits of irregular size (**Figure 6.9 b)**. At the bottom of pit, oxygen and chlorine were present with other matrix elements showing anodic dissolution of metal. The content

of oxygen and chlorine was higher (25 and 9 wt % respectively) compared to than that of unexposed sample. Potentiodynamic plot for the sample exposed at 400℃ for 100 h, shows no distinct pitting potential, smaller pits (~25µm) were formed with increase in voltage.

Exposed at 500℃

For the samples exposed at 500℃ for 100 h, number of pitting sites increased, and the subsurface pits can also be seen along with bigger circular pits (**Figure 6.9 c**). These metastable pits grew below the surface in horizontal direction. EDS analysis of corrosion product, visible in white color, shows higher content of chlorine and oxygen (9 and 28 wt% respectively) with other matrix elements compared to the samples exposed at lower temperatures.

Exposed at 600℃

As temperature of exposure increases to 600℃, pitting density and size also increase (**Figure 6.9 d**). This type of stainless steel is prone to Cr_2N precipitation when exposed at temperatures above 500°C. This resulted in a marked rise in pit density and size. Precipitation of Cr_2N along the grain boundary results in grain boundary corrosion. Subsurface pits of around ~80 µm diameter were observed on the surface of the samples exposded at 600°C. EDS analysis of the corrosion products shows a higher amount (22.5 and 27 wt% respectively) of chlorine and oxygen with other matrix elements showing increased metal dissolution at the bottom of pits. Also, potentiodynamic plot for 100 h exposure at 600℃, shows significant increase in current density, at constant potential which shows that re-passivation of pits does not occur.

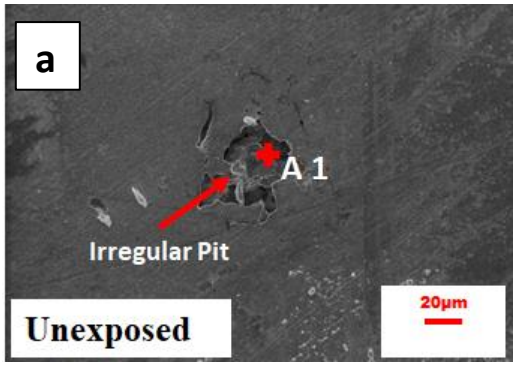

Element (wt%)	A 1
O K	13.84
Cl K	4.04
Cr K	16.47
Mn K	19.87
Fe K	45.78

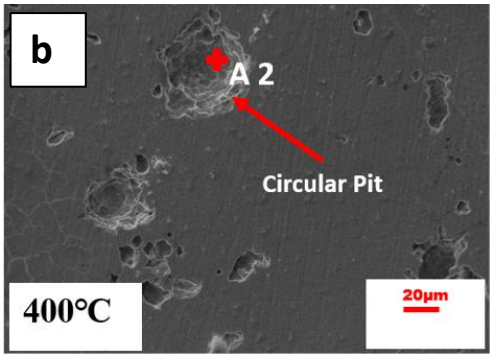

Element (wt%)	A 2
O K	25.60
Cl K	9.30
Cr K	14.73
Mn K	12.92
Fe K	37.45

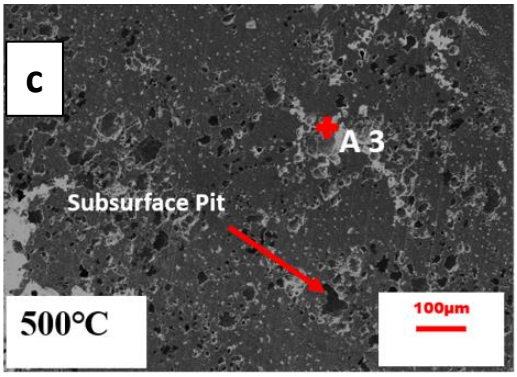

Element (wt%)	A 3
O K	28.19
Cl K	9.12
Cr K	16.53
Mn K	14.85
Fe K	31.31

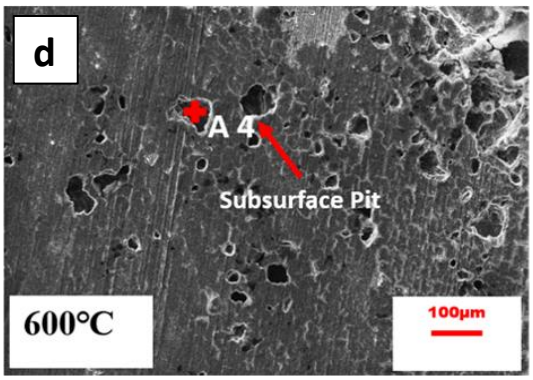

Element (wt%)	A 4
O K	27.88
Cl K	22.51
Cr K	13.09
Mn K	18.74
Fe K	25.78

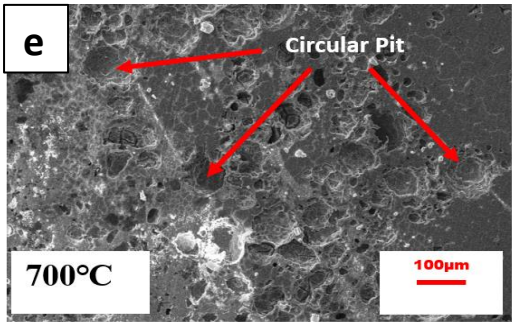

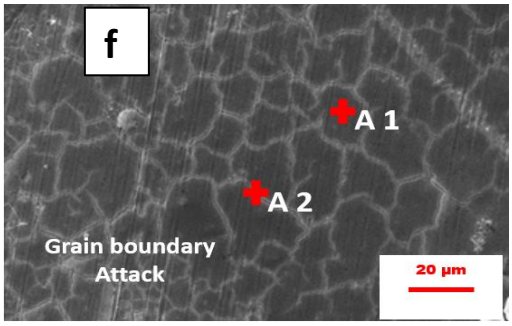

Element (Weight%)	A 1	A 2
O	13.73	15.48
Cr	16.92	16.47
Mn	20.43	20.48
Cl	16.2	21.1
Fe	32.73	26.47

Figure 6.9: SEM-EDS analysis of corroded surface of Fe-18Cr-21Mn-0.65N austenitic stainless steel samples, (a) unexposed and those exposed at (b) 400°C, (c) 500°C (d) 600°C, (e&f) 700°C for 100 h.

Exposed at 700℃

On the samples exposed at 700℃ for 100 h, severe pitting was observed along with grain boundary attack (**Figure 6.9 e** and **f**). Micrograph (**Figure 6.9 e**) shows that almost all the surface was covered with bigger pits. Shallow and circular pits with deep subsurface pits were prominent at this temperature. It was due to precipitation of Cr_2N along the grain boundaries as well as within the grains, which act as pit nucleation sites. Grain boundary attack can be seen in **Figure 6.9 f**. EDS analysis shows that at grain boundary chlorine content was higher (21 wt%) compared to bulk showing preferential attack due to anodic dissolution of metal by breaking passive layer.

6.2.3.3.2. Cross sectional Analysis of Pits

Figure 6.10 shows SEM micrographs of the pits formed after potentiodynamic corrosion test of the Fe-18Cr-21Mn-0.65N austenitic stainless steel exposed in temperature range of 400-700℃ for 100 h in 0.5M NaCl solution. Pitting action was prominent at the unexposed as well as on the samples exposed at 400-500℃, while grain boundary attack was prominent for the samples exposed at 600-700℃. **Figure 6.10** shows cross section of a pit, formed at the sample without exposure. Pit depth ranged from ~45-50 microns on the surface while a small undercut pit can also be seen in **Figure 6.10 a**. Pit formed had inverted pot like shape with a narrow opening. Metastable/small pits can also be seen at the surface. The pit depth on the sample exposed at 400° increased to 60-65 microns. A wider pit opening can be seen compared to the pit formed on the unexposed sample. **Figure 6.10 c** shows micrograph of a pit formed at the surface of the sample exposed at 500℃. It shows that as the temperature of exposure increases, the depth and width of the pits also increase. A shallow and small pit gets merged to a bigger stable pit. Disc and rod shape precipitates of Cr_2N can be seen, which increase the intensity of attack. Further increase in exposure temperature resulted in preferential intergranular attack. **Figure 6.10 d** shows the pits

formed at surface of the sample exposed at 600°C, the depth of attack was lower compared to samples exposed at lower temperatures. Precipitation of the rod shaped Cr_2N along the grain boundary can be seen which resulted in preferential attack on grain boundary. The grain boundary of grain gets dissolves preferentially where chromium nitride precipitation takes place leading to detachment of grain. From the micrograph in the circled region, it can be seen that corrosion attacks gets restricted after dissolution of precipitates. As the temperature of exposure increases to 700°C, more precipitates of Cr_2N form along the grain boundary as well as within the matrix. The samples exposed at 700°C, experienced maximum corrosion attack and fragmentation or detachment of grains (**Figure 6.10 e**). In the samples exposed at 600°C, corrosion attack gets restricted after dissolution of the precipitates along the grain boundary but in the sample exposed at 700°C, a uniform attack can be seen.

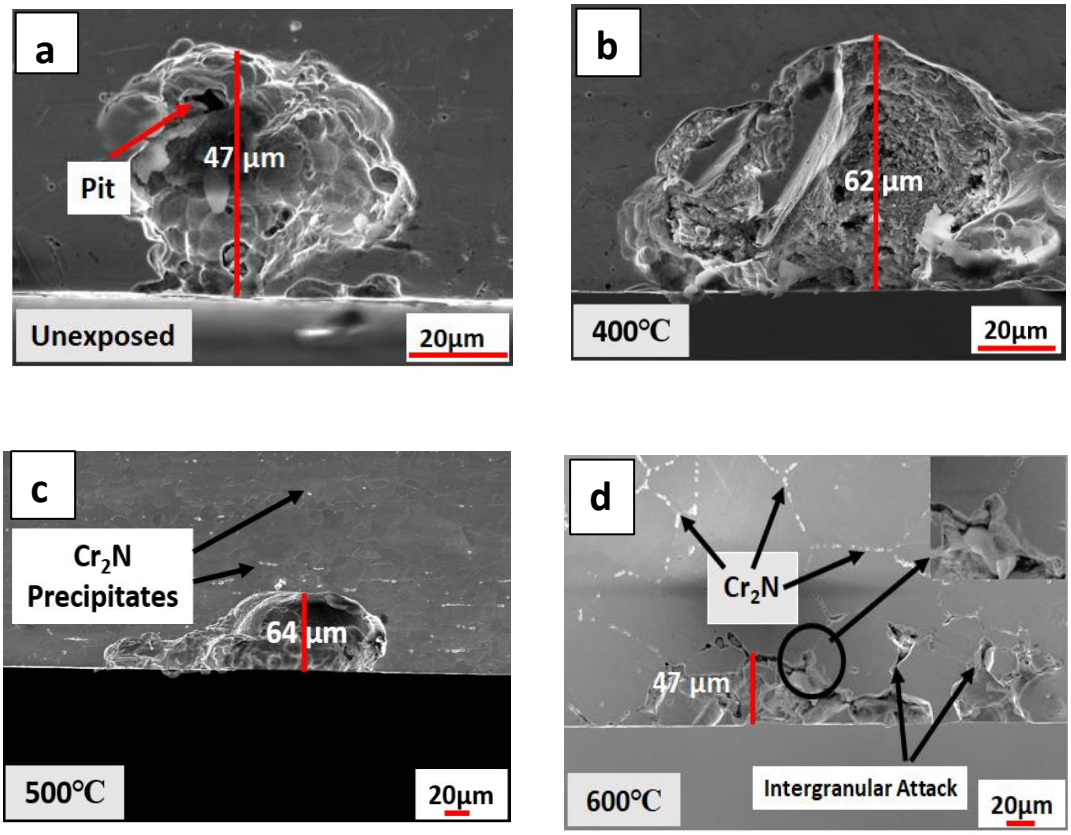

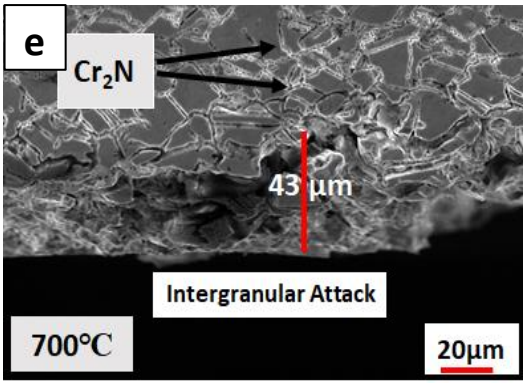

Figure 6.10: SEM micrographs of longitudinal cross sections, normal to corroded surfaces of the Fe-18Cr-21Mn-0.65N austenitic stainless steel, (a) unexposed and exposed for 100 h: at (b) 400°C, (c) 500°C (d) 600°C and (e) 700°C.

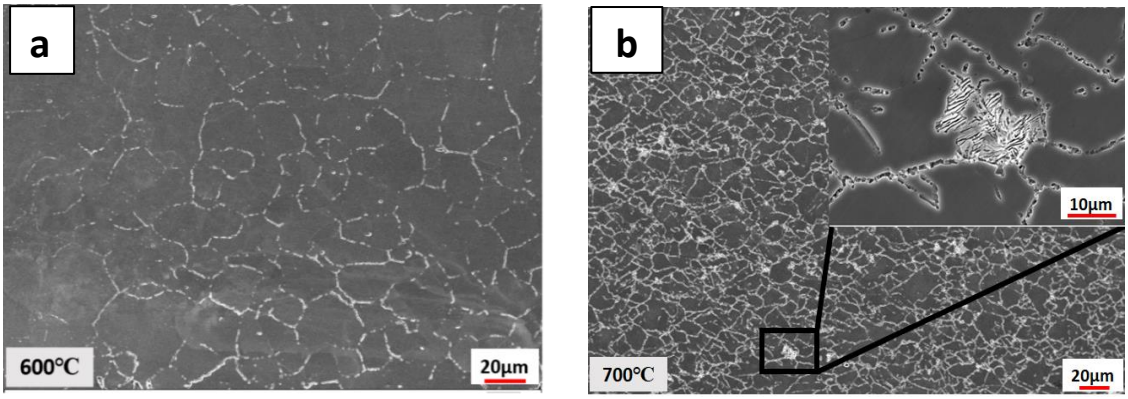

Figure 6.11: SEM micrographs of surface of the Fe-18Cr-21Mn-0.65N austenitic stainless-steel samples exposed for 100 h at: (a) 600°C and (b) 700°C.

Figure 6.11 a and **b** shows micrographs of the samples exposed at 600 and 700°C, revealing precipitation of Cr_2N. In the samples exposed at 700°C, there are lamellar precipitates of Cr_2N inside the grains and disc & rod shaped Cr_2N precipitates at the grain boundaries. In the sample exposed at 600°C, quantity of precipitation was relatively less compared to that exposed at 700°C. These two micrographs clearly show the increase in severity of corrosion and pitting at higher temperatures.

6.3. Discussion

Corrosion behavior of the exposed Fe-18Cr-21Mn-0.65N stainless steel in the temperature range of 400-700°C, with varying duration of exposure was studied in 0.5 M NaCl solution.

As shown in Chapter 3 and 5 this alloy exhibited good oxidation resistance and tensile properties at temperatures up to 500℃, after 100 h of exposure [153].

6.3.1 EIS Study

EIS study of the sample exposed for 100 h, in the temperature range of 400-700℃, shows that exposure reduces the resistance of passive film against chloride corrosion (**Figure 6.1**). The sample exposed was found more resistant to chloride attack compared to those exposed from 400-700°C. The unfinished semicircular arc in Nyquist plot (**Figure 6.1 a**) and sigmodal Bode plots (**Figure 6.1 b** and **c)** clearly show that as the temperature of exposure increases, the resistance of passive film against corrosion decreases, due to the internal microstructural change. Precipitation of Cr_2N at higher temperature of 500-700℃ causes segregation of Cr at the grain boundary, which results in depletion of Cr and formation of discontinuous passive layer [15, 80]. From Table 6.1, it is clear that the resistance of passive film directly influences the corrosion property, it decreases with increase in temperature of exposure. Precipitation of Cr_2N along grain boundary and inside the grain causes formation of discontinuous chromia layer, resulting in direct contact of chloride ions with the less protective oxide film of iron and manganese. EIS gives the primary idea about the ability of the passive film, to resist corrosion attack. It was further studied by potentiodynamic polarization test to examine the behavior in chloride environment.

6.3.2 Potentiodyanmic Polarization Test

Effect of exposure time and temperature on corrosion behavior can be seen in **Figure 6.3**, the related parameters are given in Table 6.2. It is evident that exposure time and temperature directly influence the corrosion parameters. It can be seen from the corrosion plot (**Figure 6.3a**), that the unexposed sample has lower E_{corr} value and higher resistance to polarization due to formation of a protective passive film at the surface. The curve does not show steep increase in the current density which signifies that the pits were metastable.

It should be noted from **Figure 6.3** that there was no distinct demarcation of pitting potential at all temperatures and exposure time. The shape of the curve of the sample exposed at 400℃ was similar for all the exposure time. It gets shifted towards right with increase in time, suggesting a higher corrosion rate of the specimens exposed for 100 h. Further increase in exposure time at 500 ℃, changes the shape of polarization curve (**Figure 6.3b**). Here, at all the temperatures of exposure, a steep increase in current density can be seen which is due to increase in the amount of Cr_2N precipitates along the grain boundary (**Figure 6.10c**). It can be seen from Table 6.2 that increase in exposure time increases the corrosion rate at all the temperatures of exposure. The polarization curve (**Figure 6.3 c**) gets shifted downwards, and towards the right side, indicating increase in corrosion rate. At 100 h of exposure, a steep increase in corrosion current can be seen, possibly due to precipitation of chromium nitride along grain boundary. As temperature of exposure increased to 600℃, similar behavior was observed. Rod like precipitates can be seen at the grain boundary which act as active corrosion sites. Intergranular attack results in a steep increase in corrosion rate, at higher exposure of 100 h (**Figure 6.3d**). This shape of curve depicts that after the cathodic region, corrosion starts rapidly. Further increase in exposure temperature to 700℃ for 100 h of exposure resulted in a steep increase in the current density, which was attributed to increase in the quantity of precipitates along the grain boundary as well in the grains (**Figure 6.11 b**). A steep increase in corrosion current density had a direct relation with the dissolution lamellar Cr_2N formed, during the exposure. The mechanism of corrosion is explained in the section 6.3.4 of this chapter.

6.3.3 Surface layer analysis

XPS analysis gives an idea about the composition of the corrosion product / passive layer after the corrosion. It also reveals the role of each element in the matrix and its dissolution. From the XPS plots in **Figure 6.5-6.8**, it can be seen that the passive layer formed at the

surface contains Fe, Mn, Cr and O in it. The intensity of Fe and oxygen was highest at all temperatures of exposure which shows that the passive layer is composed mainly of Fe and O (**Figure 6.6** and **6.8**). Fe $2p_{3/2}$ contains Fe^{+3} with oxide and hydroxide attached to it. Metal dissolution starts from dissolution of the passive layer formed at the surface. During potentiodynamic polarization test, reaction 6.1 occurs at anode where release of electron at anode occurs which disturb the equilibrium. The released electrons result in formation of hydroxyl ions (reaction 6.2) from the aqueous solution which further results in formation of various oxides and hydroxide according to reactions 6.3 and 6.4. Sodium chloride in the aqueous solution gets dissociated and Cl^- ions form different metal chlorides such as of Fe and Cr, according to reactions 6.1 and 6.10 [81].

$$Fe \rightleftharpoons Fe^{+3} + 3e^- \quad (6.1)$$

$$2H_2O + O_2 + 4e^- \rightleftharpoons 4OH^- \quad (6.2)$$

$$2Fe^{+3} + 3O^{-2} \rightleftharpoons Fe_2O_3 \quad (6.3)$$

$$Fe^{+3} + 2OH^- \rightleftharpoons Fe(OH)O + e^- \quad (6.4)$$

$$Fe^{+3} + 3Cl^- \rightleftharpoons FeCl_3 \quad (6.5)$$

$$2FeCl_3 + 3H_2O \rightleftharpoons Fe_2O_3 + 6HCl \quad (6.6)$$

Cr $2p_{3/2}$ of unexposed sample shows presence of Cr^{+3} ion which combines with oxygen to form Cr_2O_3, gets hydrolyzed during chloride ion attack. Some of the possible chromium reactions which can occur during the potentiodynamic polarization test are given below:

$$Cr \rightleftharpoons Cr^{+3} + 3e^- \quad (6.7)$$

$$2Cr^{+3} + 3O^{-2} \rightleftharpoons Cr_2O_3 \quad (6.8)$$

$$Cr^{+3} + 2OH^- \rightleftharpoons Cr(OH)O + e^- \quad (6.9)$$

$$Cr^{+3} + 3Cl^- \rightleftharpoons CrCl_3 \quad (6.10)$$

$$2CrCl_3 + 3H_2O \rightleftharpoons Cr_2O_3 + 6HCl \quad (6.11)$$

$Mn2p_{3/2}$ spectra show the presence of Mn^{+2} and Mn^{+3} with oxide, since manganese exhibits different valence states, it can easily lose electrons to form different oxides with other matrix elements such as Fe and Cr. As shown in Chapter 3, Mn tends to combine with oxides of different matrix elements, and formation of complex spinel cannot be ignored [81, 154, 155]. The probable reactions of Mn in the present case are summarized below.

$$Mn \rightleftharpoons Mn^{+3} + 3e^- \quad (6.12)$$

$$2Mn^{+3} + 3O^{-2} \rightleftharpoons Mn_2O_3 \quad (6.13)$$

$$Mn^{+3} + 2OH^- \rightleftharpoons Mn(OH)O + e^- \quad (6.14)$$

XPS plots of the unexposed and corroded samples clearly show that iron and chromium hydroxide were formed along with their oxides by the reactions 6.4 and 6.9. On the samples exposed at 400°C, formation of hydroxide of Mn takes place along with those of Fe and Cr according to reactions 6.4, 6.9 and 6.14. Dissolution of chromium nitride occurs at higher applied potential, as discussed by K L Chao et. al. l [81]. Since Cr and N have weak bonds and Cr has higher hydration ability, it results in formation of NH_3 and NH_4^+ according to the reactions given below.

$$[N] + 4H^+ \rightleftharpoons NH_4^+ \quad (6.15)$$

$$2Cr_2N + 3H_2O \rightleftharpoons 2Cr_2O_3 + 2NH_3 \quad (6.16)$$

These NH_4^+ and NH_3 in the solution also enhance the precipitation of Mn hydroxide (Mn (OH)O) from the aqueous solution, in solid form [156]. It should be noted that the presence of ammonium ions in aqueous solution also enhances the precipitation of hydroxide of other matrix elements as well but the free energy of formation of manganese hydroxide is lowest which causes preferential precipitation of the same [157-159]. Further increase in temperature of 500°C led to formation of hydroxide of Mn, Fe and Cr, according to reaction 6.14, 6.9 and 6.4. Increase in dissolution of Cr_2N for the samples exposed at above 500 °C

according to reactions 6.15 and 6.16 causes increase in precipitation of Mn hydroxide. Samples exposed at above 600℃, the amount of precipitation increases and their dissolution leads to higher quantity ammonium ions in the vicinity of pits. This promotes formation of Mn hydroxide compared to iron. It can be seen from $Cr2p_{3/2}$ spectra for the samples exposed at 600℃, chromium oxide and hydroxides were present. On increasing the temperature to 700℃, precipitation increases along the grain boundary as well as inside the grains. A uniform attack along the grain boundary results in detachment of grains from the matrix to solution. Metallic Fe^0, Cr^0 and Mn^0 peaks were observed in the specimens exposed at 700℃ which was the consequence of uniform attack (**Figure 6.5e**, **6.6e** and **6.7e**). Also, it shows that a very thin passive layer was formed at 700℃.

6.3.4 SEM-EDS analysis

SEM morphology (**Figure 6.9** and **6.10**) shows that pitting was prominent at all the temperatures of exposure, in 0.5M NaCl solution, although no clear demarcation of pitting potential was observed from the potentiodynamic plots (**Figure 6.3**). It is seen clear from the SEM micrograph that pitting was not uniform and corrosion attack changed from pitting to intergranular. Also, the density and size of the pits increased with rise in the exposure temperature. Circular and irregular morphologies of pits were observed in the samples exposed at different temperatures. Pitting starts when a thin passive layer of chromia gets damaged chemically/ mechanically. At the damaged site, formation of deep cavities takes place which signifies the anodic reaction (6.4, 6.7 and 6.12). These cavities in presence of chloride ions, act as an electrochemical cell by disturbing the local equilibrium. Based on surface inhomogeneities and microstructural changes the extent and shape of pitting can be estimated [159, 160]. During pitting, discrete localized surface undergoes attack while remaining surface is not affected. At room temperature, an irregular shape pit can be seen from the micrograph (**Figure 6.9 a**) which was attributed to the localized thinning or

dissolution of chromia layer according to reaction 6.9 and matrix elements such as iron and manganese get directly exposed to the aqueous solution. Cross section micrographs of the surface undergone pitting show subsurface growth of pit (**Figure 6.10 a**). As the temperature of exposure increased to 400 and 500℃, multiple pits sites can be seen in the micrographs (**Figure 6.9 b**). This was consequence of chromium segregation / precipitation along the grain boundary [153, 161]. Precipitates act as nucleation site for pits to grow. Further, in increase in voltage results complete dissolution of these precipitates causing increase in ammonium content in the vicinity of pit. This results in more severe precipitation of hydroxyl of Cr, Fe and Mn at the pit opening. It increases acidity in the vicinity of the pits resulting in the growth of pits formed. The cross section of the surface undergone pitting shows a wide and deeper pit formed (**Figure 6.10 b**). As the temperature of exposure increases to 500℃ the number density and size of pits increase (**Figure 6.9 c** and **6.10 c**). The amount of Cr_2N also increases with the temperature which results in more severe pitting. Cross section micrograph of pit for the samples exposed at 500℃, exhibiting pitting, reveals that the pits were wider and deeper compared to those of the sample exposed at 400℃. Coalescence of two pits can be seen when the pit grows horizontally due to selective dissolution of precipitates. In the sample exposed at 600 and 700℃, quite a different attack can be seen from **Figure 6.10 d** and **e**. Precipitation of Cr_2N along the grain boundaries as well as in grains enhanced the intergranular corrosion and (**Figure 6.11 a** and **b**) and similar results were observed also elsewhere [162]. Pitting of samples can also be seen in the micrographs of the sample exposed at 600℃. This was due to the fact that precipitation was not uniform as in the case of the samples exposed at 700℃ (**Figure 6.9 e**). The cross section of the samples exposed at 600℃ showed intergranular attack. The dissolution of Cr_2N was preferential (inset of **Figure 6.9 d**). The cross section of the samples exposed at 700℃ reveals a uniform attack along the grain boundary which results

in detachment of grains from the matrix. This type of attack was shallow but more material was lost compared to pitting attack due to uniform corrosion.

6.3.5 Mechanism of Corrosion

Based on the present study, the mechanism of chloride corrosion of the 'nickel free' high Mn nitrogen stabilized austenitic stainless steel unexposed and exposed from 400-700°C for 100 h can be divided into two regimes:

Regime I: Pitting corrosion of the specimens exposed up to 500°C

Pitting corrosion in two steps occurred, in the first step by dissolution/ breakage of passive film and in the second step by formation and growth of pits. Dissolution of passive film under high electric field strength occurs by adsorption/ penetration of Cl^- ions on the passive film which is composed of porous layer and surface barrier film in the present study. Cl^- ions replace the oxides and hydroxides in the passive film in anodic range at sufficient positive potential. This causes breakdown of passive film by electrostriction due to penetration of chloride ions. Cl^- ions can also penetrate through the lattice of passive layer via defects. The exchange of aggressive Cl^- ions with O^{-2} and OH^- ions from the passive film generates cation/metallic vacancies which further enhances the diffusion of chloride ions to the metal/film interface. Accumulation of these metallic vacancies causes formation of voids resulting in collapsing of the passive film [31, 163]. Breakdown of passive film leads to formation of localized perturbations which causes initiation of pits. This process can occur throughout the surface which is exposed to electrolyte, but pits formation only can take place where the repair of passive film cannot occur [164]. This behavior can be seen in **Figure 6.3**.

Second step is pitting which is categorized into three steps: first nucleation of pits in which later sites act as pit nucleation sites. Reactions 6.1, 6.7, 6.12 and 6.13 occur in anodic region

which cause release of metal anions into the electrolyte. At cathodic end/ at electrolyte metal interface reaction 6.2 occurs leading to formation of an electrolytic cell. Further, increase in potential leads to second step which is the growth of pits and in this step the local acidity inside the pits increases. Reactions 6.5, 6.6, 6.10 and 6.11 occur during this process. Due to hindrance in diffusion of OH^- ions local acidity of pits increases. Third step is stabilization of pits where system attains equilibrium by diffusion of OH^- ions inside the pits. A schematic representation of pitting at room temperature can be seen in **Figure 6.12 a**. At the temperature of 400 and 500°C, pitting mechanism was similar to that at room temperature, the only difference was that nucleation sites of pits increased.

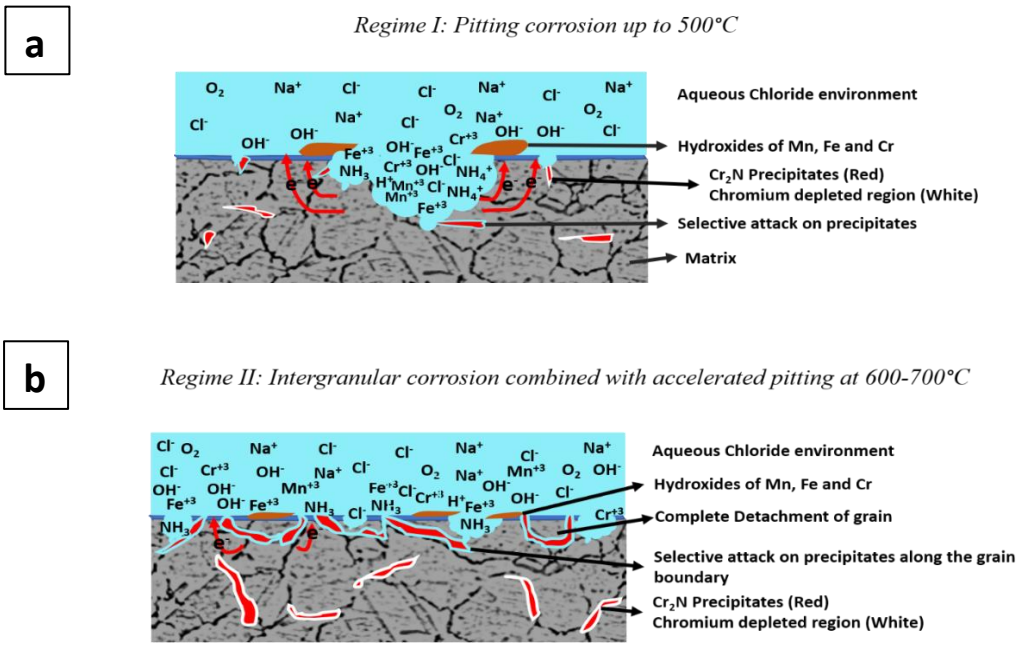

Figure 6.12: Schematic mechanism of corrosion for the Fe-18Cr-21Mn-0.65N austenitic stainless steel samples, (a) unexposed, and exposed at 400-500°C, (b) exposed at 600-700°C for 100 h.

Multiple pitting sites cause acceleration in process of metal dissolution. Also, at these temperatures reactions 6.15 and 6.16 occurred which caused preferential precipitation of manganese hydroxides at the surface from the electrolyte.

Regime II: Intergranular corrosion combined with accelerated pitting at 600-700°C

Exposure of samples at 600-700°C resulted in sensitization of the steel due to the precipitation of harmful chromium nitrides. Dissolution of passive film was followed by intergranular and pitting attacks. In the samples exposed at 600 and 700℃ for 100 h, intergranular attack was prominent due to abundance of Cr_2N along the grain boundary as shown in **Figure 6.12 b**. In the intergranular attack, chromium deficient region, adjacent to grain boundary on both sides act as attack site. Depletion of Fe^{+3} and Mn^{+3} starts according to anodic reactions 6.1 and 6.12. A complete dissolution of Cr_2N leads to detachment of grain from the matrix. This type of attack is more severe and leads to more metal dissolution. Dissolution of chromium nitride according to reaction 6.16 promotes the precipitation of manganese hydroxides from the electrolyte.

6.4. Conclusions

The effect of intermediate temperature exposure at 400-700℃ for 100 h on corrosion behavior of the "nickel free" Fe- 18Cr-21Mn-0.65N austenitic stainless steel was studied in 0.5 M NaCl solution. The results are compared with solution annealed samples (unex). Following are the major conclusions:

1. Potentiodynamic polarization corrosion test showed that higher temperature of exposure and long duration of exposure decrease corrosion resistance of the surface passive layer. This steel showed susceptibility to chloride corrosion following exposure at 400 -700℃ as well as in the unexposed condition. The corrosion rate increases with temperature and time of exposure.

2. Chloride ions induced corrosion attack can be correlated with the precipitation of harmful Cr_2N in the material. Exposure at the temperature of 600-700°C for 100 h resulted in preferential intergranular corrosion due to enhanced precipitation of Cr_2N.

3. The mechanism of corrosion for this kind of steel can be divided into two regimes. The first regime of pitting induced corrosion up to 500°C of exposure and the second regime of intergranular corrosion combined with accelerated pitting from exposure at the temperature of 600-700°C.